CrossMark

ORIGINAL PAPER

Investigation of amino acids as templates for the sol–gel synthesis of mesoporous nano TiO$_2$ for photocatalysis

Pratibha V. Bakre[1] · Santosh G. Tilve[1,2] · Naren N. Ghosh[3]

Abstract TiO$_2$ nanoparticulates of well-defined size were synthesized using amino acid templates employing sol–gel method. Eight different amino acids were studied. The samples were characterized by various methods such as X-ray diffraction, Fourier transform infrared spectroscopy, ultraviolet–visible diffuse reflectance spectroscopy, Brunauer–Emmett–Teller surface area measurement, and transmission electron microscopy. Of the amino acids used, catalyst employing aspartic acid was found to have minimum particle size of 10.4 nm and maximum surface area of 95.3 m^2/g. The catalytic activity of the prepared TiO$_2$ samples was compared with Degussa-P25 catalyst for direct sunlight photodegradation of methylene blue and calmagite dyes. Catalyst prepared form branched amino acids, proline, valine, and aspartic acids, were found to give better results. Based on infrared spectroscopy studies, it is proposed that amino acids act as a surfactant by hydrogen bonding between the hydrogen of the ammonium ion and the surface hydroxyl group of the colloid.

Graphical abstract
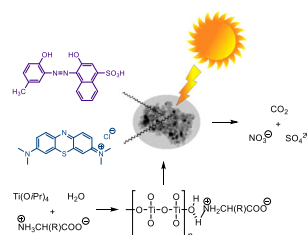
Keywords Methylene blue · Calmagite · Catalyst · Photodegradation · Nanochemistry

Introduction

Inorganic semiconductor metal oxides have attracted extensive attention in the field of environmental chemistry for the photocatalytic decomposition of organic pollutants in the air and water [1–10]. Among the many materials TiO$_2$ is one of the most studied and an important technological material that can be used for photocatalysis and other applications such as pigments, UV blockers, optoelectronics, dye sensitized solar cells, Li-ion batteries, etc., because of its advantages of low cost, non-toxicity, high activity, and long durability [11–15].

Recently, the construction of TiO$_2$ hierarchical materials with different morphologies has attracted much attention worldwide [16–31]. The efficiency of the oxide in each of those applications depends on the phase, size, and shape of the particles used [8–10, 32–34]. It is well known that the anatase polymorph displays a higher photocatalytic activity than the rutile and brookite [35, 36]. In addition to

✉ Santosh G. Tilve
stilve@unogoa.ac.in

1   Department of Chemistry, Goa University, Goa, India

2   Organic Chemistry Department, RUDN University, 6 Miklukcho-Maklaya Str., Moscow 117198, Russian Federation

3   Nano-Materials Lab, Department of Chemistry, Birla Institute of Technology and Science Pilani, KK Birla Goa Campus, Goa, India

 Springer

morphologies, the specific surface area (S_{BET}) and pore structure are also important factors for photocatalytic applications [37–40].

Present study was directed to prepare a mesoporous nano TiO_2 material as a photocatalyst for a practical environmental remediation using direct sunlight. Among the various methods used for the preparation of these materials such as hydrothermal, solvothermal, sol–gel, combustion, etc., sol–gel method was chosen for its simplicity of the procedure. Along with the method, the template material used for the preparation also plays an important role in improving these properties. It was felt that amino acids, the natural building units of proteins, could serve as a smart template in the preparation of mesoporous nano TiO_2 materials with desired structure and surface properties.

Amino acids have been routinely used in the combustion and solvothermal synthesis of TiO_2 [41–54]. However, a direct comparison of the amino acids for the sol–gel synthesis of nano TiO_2 is lacking. Organic acids in general reacts with the surface hydroxyl groups of the metal oxides and forms a metal carboxylate bond and thereby control the condensation of the sol to restrict the size of the particles. Amino acids exist in zwitterionic forms and they are expected to behave differently than the other organic acids. However, the same is not studied in detail about the amino acids. Some of the reports suggested that amino acids act as a template by reacting with surface hydroxyl group and forms metal carboxylates [55–57], while one report suggested adsorption of an amino group on the surface of TiO_2 [58]. We were also interested to know the role of amino acids in controlling the size of the particulate in the sol–gel synthesis of TiO_2 and thereby their effect on the photocatalytic properties of the catalyst formed.

We had recently reported that chain length of the aliphatic acid template significantly affect the size, phase, and the mesoporosity of the TiO_2 catalyst during sol–gel synthesis [59]. In the present work, the synthesis of mesoporous TiO_2 nanoparticles using amino acid templates is described. Amino acids are best suited as templates as they are biological building units in proteins. A series of the amino acids, glycine, DL-alanine, β-alanine, DL-valine, L-proline, DL-serine, DL-aspartic acid, and L-glutamic acid (Table 1) in water were treated with a titanium isopropoxide solution. The resulting TiO_2 nanoparticles were studied for photocatalytic activity in comparison with reference material, Degussa P25.

Textile, cosmetic, paper, drug, and food processing industries use synthetic organic azo dyes in large quantities. Their discharge into the environment and its subsequent effects is of major concern. Methylene blue (MB) is commonly studied azo dye due to its complex aromatic structure and harmful intermediates. But not much work is found on the similar azo dye calmagite (3-hydroxy-4-(2-hydroxy-5-methylphenyldiazenyl)naphthalene-1-sulfonic acid). The synthesized catalysts were studied for the photocatalytic degradation of this dye along with MB. The catalysts prepared are labelled as follows (Table 1).

Results and discussion

IR spectroscopy

The IR spectra of all the calcined TiO_2 samples show a typical absorption band for Ti–O–Ti network as a strong, broadband around 600 cm^{-1}. A slightly less strong, broadband at 3300–3500 cm^{-1} (O–H stretching mode) and weak bands at $\sim$1633 cm^{-1} seen were due to physically adsorbed water on the surface of TiO_2 and surface hydroxyl groups (Fig. 1a). In the spectra of precursor samples (Fig. 1b), the strong, broadband between 2500-3500 cm^{-1} (R–COOH) and four typical strong bands between 1400–1600 cm^{-1} (C=O$_{(s,un)}$, −NH$_3^+$,−CH$_2$) suggested the presence of unreacted amino acids. The close resembles of these spectra with the starting amino acids' spectra with no significant change in the region 1400–1600 cm^{-1} suggested absence of metal carboxylates bonds [45]. Such a metal carboxylate bond is usually formed when organic acids are heated with Ti(OH)$_4$. This was further confirmed by mixing Ti(OH)$_4$ and glycine and heating at 100 °C which displayed a similar IR spectrum. This was also further studied by heating the precursor sample of glycine at different temperatures viz. 200, 300, and 400 °C (Fig. 1c). The IR spectra of the sample heated at 200 °C did not show any remarkable change while the sample heated at 300 °C showed the presence of a strong band at 1683 cm^{-1}, which could be due to the presence of the free carboxylic acid group (Scheme 1). The IR spectrum of sample heated 400 °C was matching with the calcined sample C1. TG–DTA of the precursor sample (Fig. 1d) also showed similarity with the reported TG–DTA of

Table 1 List of precursor amino acids and catalyst labels

Precursor acid	Label
Glycine	C1
L-Proline	C2
β-Alanine	C3
DL-Alanine	C4
L-Glutamic acid	C5
DL-Aspartic acid	C6
DL-Valine	C7
DL-Serine	C8

Fig. 1 **a** IR spectra of calcined samples; **b** IR spectra of precursor samples; **c** IR spectra of precursor sample of glycine heated at different temperature; **d** TG–DTA spectra of glycine
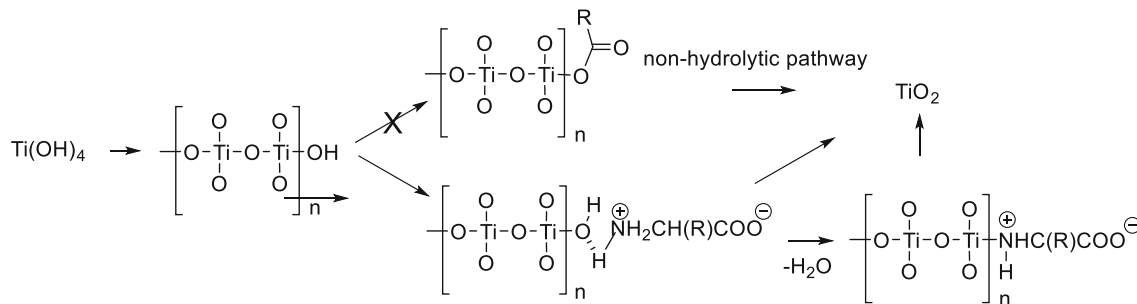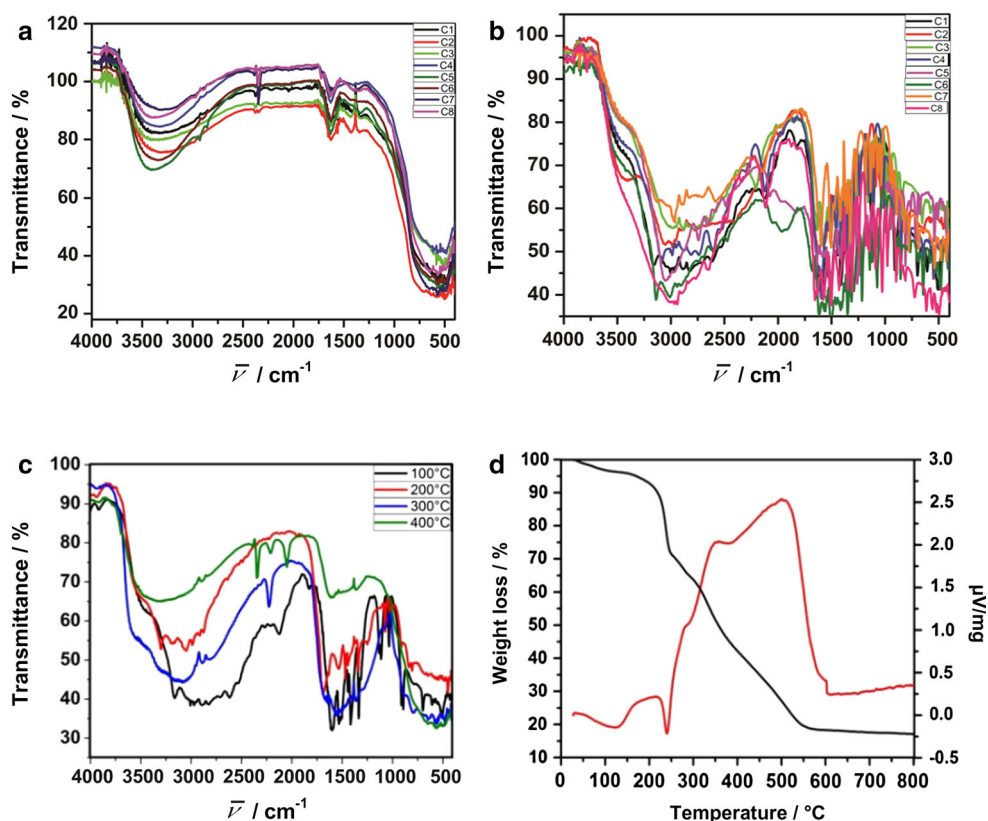
Scheme 1 .

glycine [60] confirming our observation that amino acids are more probably acting as surfactants and not as reactants [58]. In addition, precursor sample of C1 when washed with water did not show any residual carbonyl functionality while precursor sample prepared from acetic acid [59] did show the unsymmetrical and symmetrical stretching bands of the carbonyl functionality in its IR spectrum. This result could also explain why amino acids fail to functionalize TiO₂ while N-Boc amino acid could [61]. During the condensation of the Ti(OH)₄ to form nano TiO₂, the hydrogen of the ammonium group of the amino acid forms hydrogen bonding with the free surface OH groups of the particulate as shown in Scheme 1 to control the polymerization. The same phenomenon perhaps can be used to

explain the adsorption behaviour of the amino acids on the surface of TiO₂ [62].

Optical study

The optical properties of TiO₂ nanoparticles were investigated by UV–Vis diffuse reflectance spectroscopy, as shown in Fig. 2. The band gap energy (E_g) of all the synthesized samples is estimated from the intercept of UV–Vis spectra using the equation:

$$E_g = 1239.8/\lambda_{max}$$

where E_g is the band gap (eV) and λ (nm) is the wavelength of the absorption edges in the spectrum.
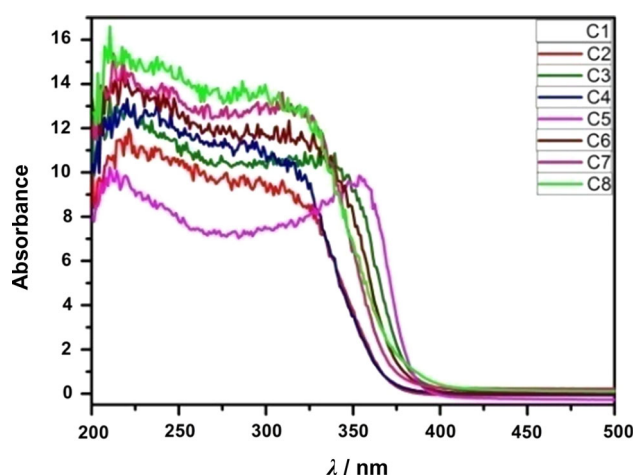
Fig. 2 UV–DRS spectra of calcined samples

From the absorption spectra, it is observed that absorption of the samples is in the UV region, confirming their wide band gap which is the range between 3.1 and 3.3 eV. The slight shift in the absorption edge observed had no significant effect on the photodegradation studies.

Crystal structure

To establish the crystallinity, crystalline phase, and the crystallite size of the pure titania nanoparticles, the analysis of the calcined nanoparticles was carried out by X-ray powder diffraction patterns (XRD). The results are shown in Fig. 3. All the samples show well resolved and sharp peaks indicating high crystallinity and the presence of small sized nanocrystals. The peak positions can be assigned to anatase TiO$_2$ (JCPDS card # 21-1272). The diffraction peaks at 25.17°, 37.65°, 47.96°, etc. are consistent with the (101), (004), (200) peaks of anatase TiO$_2$
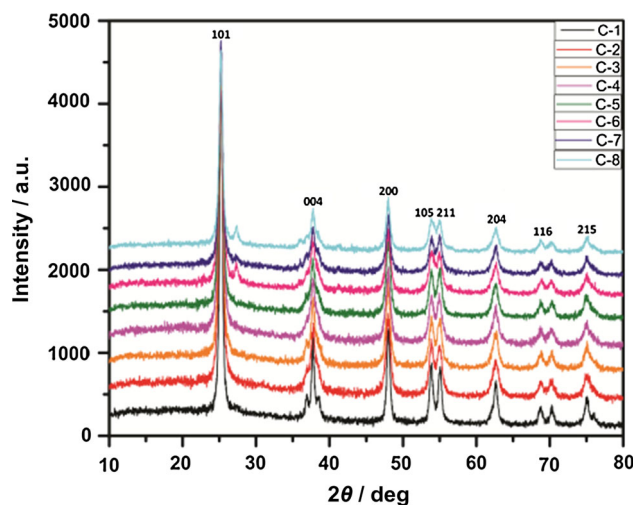

Fig. 3 XRD plots for calcined samples

for the samples C1–C5 and C7. Thus, a pure anatase phase is observed in these samples and no peak is attributable to other TiO$_2$ crystalline phases, suggesting the high purity of the samples [63]. However, the samples C6 (aspartic acid) and C8 (serine) show some percentage ($\sim$8%) of rutile phase formation. In general, branched amino acids gave samples with smaller crystallite size.

The average crystallite size for the series of TiO$_2$nano powders was determined from (101) diffraction peak (the most predominant highest intensity peak), according to the Scherrer's equation

$$D = K\lambda/\beta\cos\theta$$

where K is the Scherrer constant, λ is the X-ray wavelength, β is the peak width at half maximum, and θ is the Bragg's diffraction angle.

It is found to be in the range of 11–18 nm (Table 2). The smallest crystallize size is observed for sample C6 (aspartic acid) of 12 nm and the largest for sample C1 (glycine) of 18.9 nm. The synthesized samples were found to be smaller in size as compared to Degussa P25 [64].

Surface area and pore structure

Figure 4 illustrates the nitrogen adsorption–desorption isotherms and corresponding pore size distribution curves (inset) of the synthesized TiO$_2$ photocatalysts. The isotherms of these photocatalysts exhibited the typical IUPAC type-IV pattern with type-H3 hysteresis loop [64]. This hysteresis loop behavior can be attributed to the existence of mesopores in the size range 2–50 nm. In addition the observed hysteresis loops shifts to the higher relative pressure region, which shows the capillary condensation is associated with large pore channels [65]. The sharp decline in desorption curve is indicative of mesoporosity while hysteresis between the two curves demonstrates that there is a diffusion bottleneck, possibly caused by non-uniform pore size.

A slight variation in the shape of the hysteresis loop is observed. However, it does not show any major effect on the properties of the catalysts. The pore size distribution obtained from the desorption branch of isotherms was relatively narrow and mono modal revealing the homogeneous pore size of the samples. The specific surface area calculated from the BJH desorption plot and pore diameter of all investigated photocatalysts are summarized in Table 2. The maximum surface area of 95.3 m^2/g was observed for the sample C6 obtained from aspartic acid and a minimum of 24.6 m^2/g for the C7 (valine) sample. These results are difficult to correlate with the hydrophobic carbon chain length of the amino acids and may have to do with the affinity of the amino acids to the various surfaces of the particulate.

Table 2 Summary of the properties of TiO$_2$ nanoparticles

Sample	Crystallite, size/nm	Particle, size/nm	Average pore, diameter/nm	BJH surface, area/m^2 g^{-1}	Rate constant, K/min^{-1} for	
					MB	Calmagite
C1	18.9	15.2	10.2	47.6	0.022	0.019
C2	13.7	10.8	15.5	60.4	0.029	0.024
C3	13.6	11.7	7.0	81.8	0.020	0.018
C4	12.4	11.7	12.0	67.1	0.018	0.017
C5	12.4	13.0	7.8	72.0	0.020	0.018
C6	12.0	10.4	8.7	95.3	0.030	0.028
C7	14.2	11.2	12.7	24.6	0.029	0.022
C8	15.1	15.2	16.0	33.2	0.020	0.016
P25	25.0	21.0	17.5	56.0	0.024	0.020
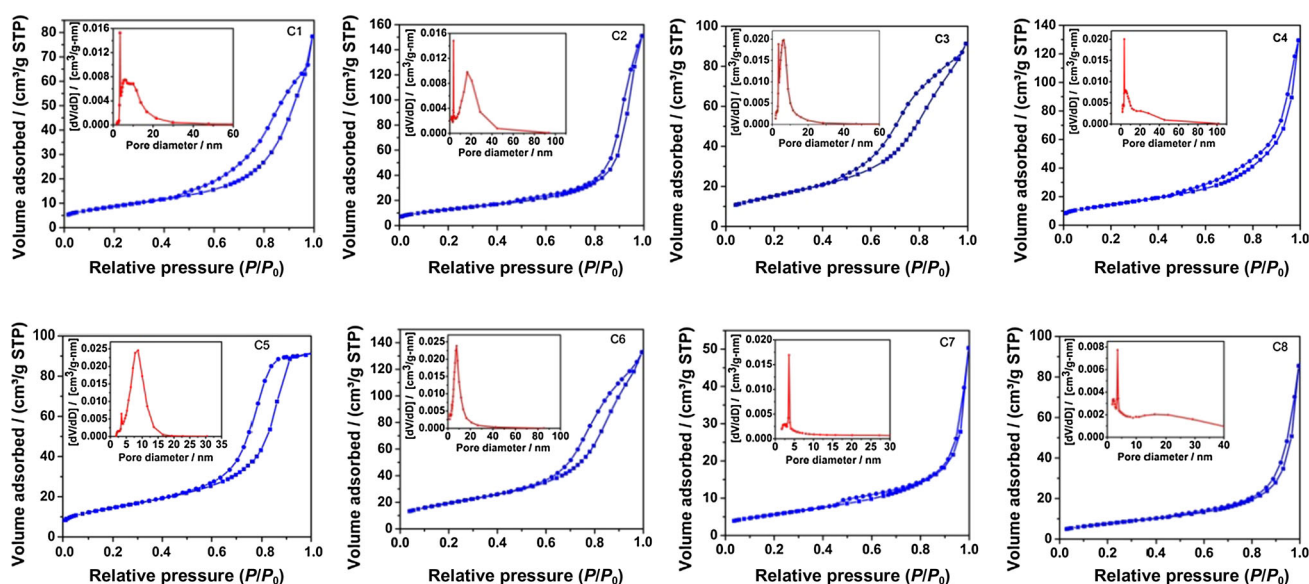
Fig. 4 Nitrogen adsorption–desorption isotherms and pore size distribution (*inset*) of TiO$_2$ nanoparticles for samples C1–C8

Morphological analysis

The exact microstructure and the particle size of the prepared TiO$_2$ catalysts were studied by TEM micrographs. The TEM images and corresponding SAED patterns are shown in Fig. 5. Largely cubical shape particles are observed with non-uniform size and some weak aggregation among the particles is also seen from TEM images. The average particle size was estimated to be about 10–15 nm, corresponding closely to the size estimated by XRD analysis. The detailed structure and crystallinity of TiO$_2$ nanoparticles can be further investigated by the SAED pattern as shown in the inset of Fig. 5. A set of diffraction rings are observed in SAED patterns due to the randomly oriented TiO$_2$ nanoparticle, which are indexed as the anatase phase of TiO$_2$, and this is consistent with the XRD results. Detailed analysis indicates that the first diffraction circle in the pattern corresponds to the (101) plane of anatase TiO$_2$. The corresponding d-spacings are assigned as (101), (004), (200), (211), (204), (220), (215), as matching with the XRD results (JCPDS no. 21-1272). Thus, it is reasonable to believe that the TiO$_2$ nanoparticles are well crystallized particles.

Photocatalytic activity

The photocatalytic activity of the samples was evaluated by their ability to degrade MB in aqueous suspensions under direct sunlight irradiation at room temperature. Direct sunlight degradation of toxic chemicals is very relevant to environmental cleansing. Figure 6a shows the concentration plots during sunlight irradiation over a time for the average results of three readings and corresponding kinetic studies. Sample C6 shows better degradation efficiency by
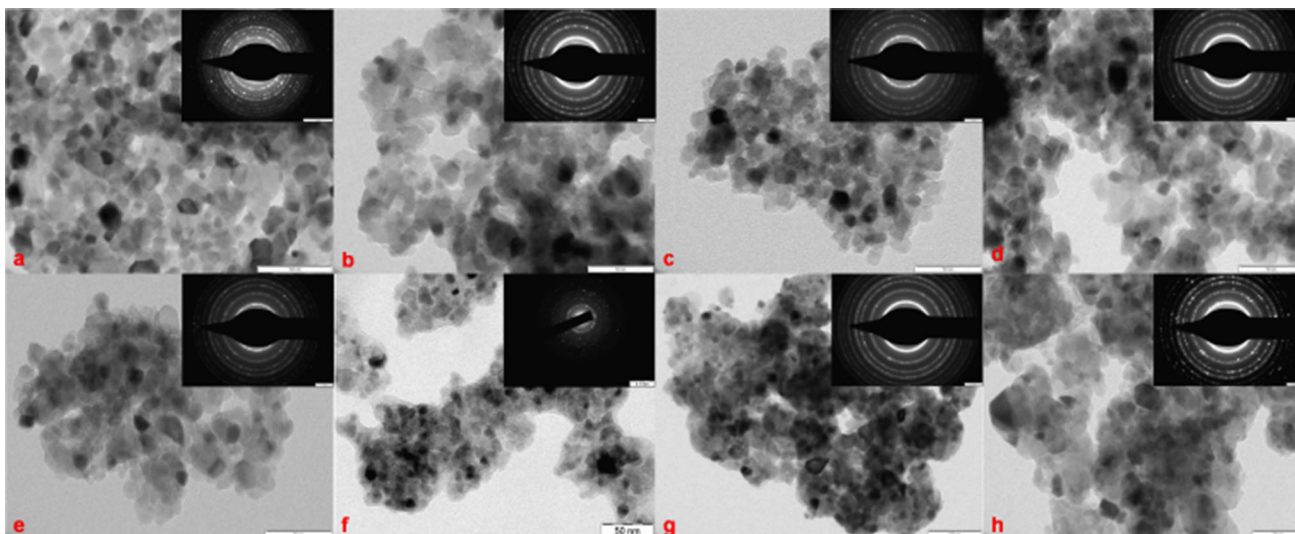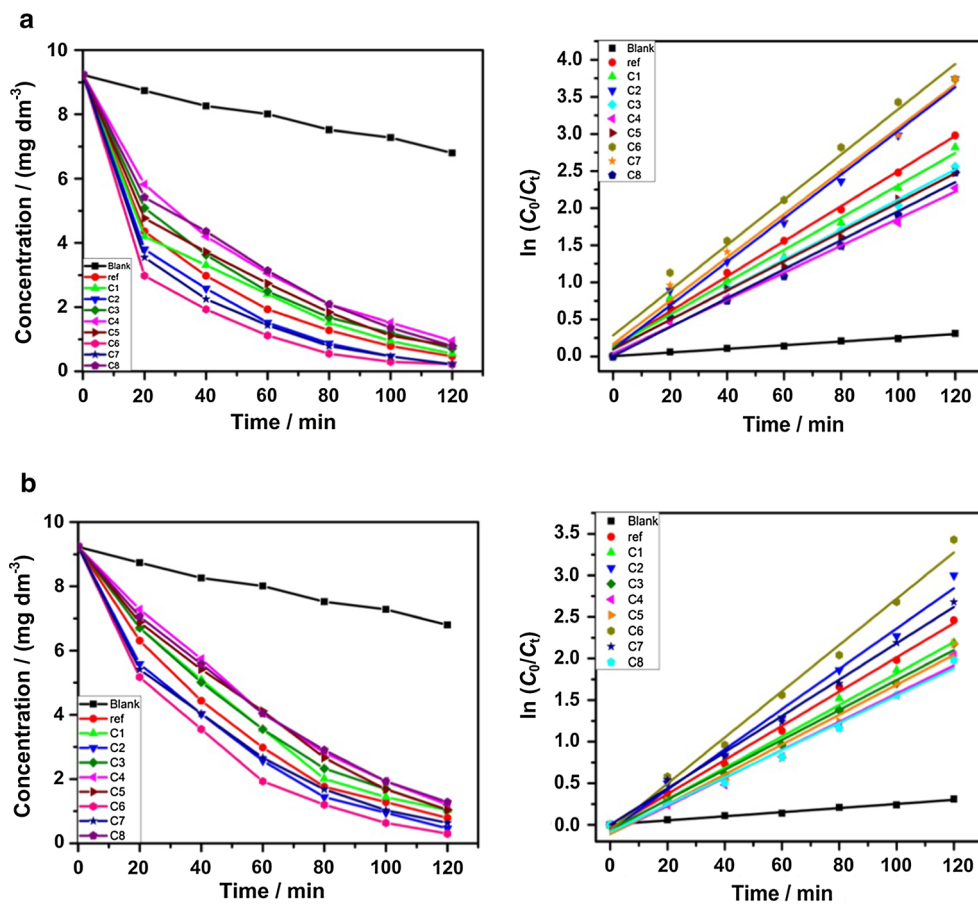
Fig. 5 TEM images of TiO_2 nanoparticles (**a–h**) and corresponding SAED patterns (*inset*) for samples C1–C8

Fig. 6 a Degradation plots methylene blue degradation and their kinetic studies; **b** degradation plots calmagite degradation and their kinetic studies

decreasing the concentration of MB at a faster rate with time, followed by sample C2 and C7, in comparison with Degussa P25.

The results were further supported by degradation of another dye, calmagite, (3-hydroxy-4-(2-hydroxy-5-methylphenyldiazenyl)naphthalene-1-sulfonic acid), an anionic azo dye where the same trend was observed. The concentration plots during sunlight irradiation of this dye and corresponding kinetic studies are shown in Fig. 6b.

The kinetics of the photocatalytic degradation reaction were studied under optimized conditions using Langmuir–Hinshelwood kinetic model

$$\ln (C_0/C_t) = kt$$

where C_0 is the initial concentration of dye solution at time $t = 0$, C_t is the concentration of dye solution after different time interval of photocatalytic reaction, and slope k is the apparent rate constant. A plot of $\ln (C_0/C_t)$ versus time (Fig. 6a, b) represents a straight line which indicates the photocatalytic degradation follows a pseudo first order kinetics. Linear relationships for all the photocatalysts is seen from which it can be observed that the apparent reaction rate constant is highest for sample C6. The rate constant k for both the dyes, is defined by $\ln (C_0/C_t) = kt$ and is given in Table 2, which is in accordance with the other results.

Thus, it is concluded here that the degradation rate depends on precursor amino acids used as a starting material. Among the acids tested, it is observed that branched amino acids give better catalyst than the straight chain compound. However, glutamic acid though have a maximum chain length of non-polar hydrocarbon chain do not give expected results and this could be due to the difference of affinity of glutamic acid compared to aspartic acid towards the surface of TiO$_2$ [55]. The little percentage of rutile phase in two samples has also not shown any significant contribution in photocatalytic activity.

Conclusions

Eight amino acids glycine, DL-alanine, β-alanine, DL-valine, L-proline, DL-serine, DL-aspartic acid, and L-glutamic acid were compared as templates for sol gel synthesis of TiO$_2$. Formation of phase pure anatase nano particulate formation was observed in all cases except aspartic acid and serine. Among these acids, particles prepared from branched amino acids proline, valine, and aspartic acid showed better photodegradation in comparison with Degussa P25 by direct sunlight exposure of dyes MB and CG. Aspartic acid was found to be the best templating agent. The smaller size of the particulate was found to be more important in determining the catalytic activity than the surface area and pore volume. Further, the IR studies suggested that the amino acids act as a template by acting as surfactant rather than the reactants. The surfactant activity was attributed to hydrogen bonding between surface hydroxyl groups of the colloid and the hydrogen of the ammonium group of the amino acids.

Experimental

Materials

Titanium tetraisopropoxide (purity 97%), Ti(OC$_3$H$_7$)$_4$, amino acids such as glycine, DL-alanine, β-alanine, DL-

valine, L-proline, DL-serine, DL-aspartic acid, and L-glutamic acid were purchased from Spectrochem, methylene blue (MB) from Merck, and calmagite (CG) from Thomas Baker. Isopropanol was supplied by Loba Chemicals was used as a solvent and deionized water was used as a medium.

Synthetic procedure

TiO$_2$ nanoparticles were synthesized by sol–gel technique, using amino acid templates, according to the method reported in our previous paper [59]. In a typical synthesis process, the absolute quantity (66.0 mmol) of an amino acid was dissolved in 200 cm^3 water and stirred to form a clear solution. Then to this solution, 16.5 mmol of titanium (IV) isopropoxide in 50 cm^3 isopropyl alcohol was added drop wise under continuous stirring at ambient temperature. A milky white suspension started developing in about 2 h. The complete gel formation was observed on stirring overnight ($\sim$12 h). The resultant white colloidal gel was dried at 100 °C to get a powder. This white precursor powder was ground and subjected to IR studies, and then calcined at 500 °C for 3 h to obtain TiO$_2$ nanoparticles.

Structural characterization

The crystal phase composition and crystallite size of the prepared TiO$_2$ nanoparticles were obtained from powder X-Ray diffractometer (Mini Flex II, Rigaku, Japan). X-ray source was Cu Kα radiation at $\lambda = 1.5418$ Å radiation at a scanning speed of 2° min^{-1}. The IR studies were carried out on a Shimadzu IR Prestige-21 FTIR in the range of 4000–400 cm^{-1}. The band gap of the samples was studied by UV–Vis diffuse reflectance spectra measured at room temperature on UV–Vis spectrophotometer (Shimadzu UV-2450). BaSO$_4$ was used as a reference material and the spectra were recorded in the range 200–800 nm. Morphologies of products and particle size were investigated by transmission electron microscopy equipped with selected area electron diffraction (TEM/SAED), using PHILIPS CM 200 field emission transmission electron microscope operating at 200 kV. Multiple point BET surface areas and pore structures were measured with a surface area and porosity analyzer (MicromeriticsTristar 3000, USA), at the temperature of liquid nitrogen. Before the analysis, samples were degassed at 200 °C for 8 h with continuous flow of nitrogen gas.

Photocatalytic activity testing

Dye stock solutions (0.010 g/dm^3 MB and 0.020 g/dm^3 calmagite) were prepared in deionized water. A given amount of the catalyst (10 mg) was added to 25 cm^3 of a dye solution. The contents of the solution were allowed to

equilibrate for a given time (usually 15–30 min) in the dark before irradiation. The samples were then irradiated in direct sunlight for 120 min between 10:00 a.m. to 12:00 noon.

After every 20 min interval, 2 cm^3 aliquots were pipetted out centrifuged and the absorbance of the clear supernatants was determined at the wavelength 660 nm for MB and at 540 nm for CG, against appropriate blanks. The kinetic studies of the same were carried out from which the rate of dye degradation was determined.

References

1. Forgacs E, Csarhati T, Oros G (2004) Environ Int 30:953
2. Zhang J, Bang JH, Tang C, Kamat PV (2010) ACS Nano 4:387
3. Kandiel TA, Feldhoff A, Robben L, Dillert R, Bahnemann DW (2010) Chem Mater 22:2050
4. Nakata K, Fujishima A (2012) J Photochem Photobiol C Photochem Rev 13:169
5. Ochiai T, Fujishima A (2012) J Photochem Photobiol C 13:247
6. Rane KS, Malsiker R, Yin S, Sato M, Kok C, Dunbar E, Biswas P (2006) J Solid State Chem 179:3033
7. Araujo PZ, Luca V, Bozzano PB, Bianchi HL, Soler-illia G, Blesa MA (2010) ACS Appl Mater Interfaces 6:1663
8. Zhao T, Liu Z, Nakata K, Nishimoto S, Murakami T, Zhao Y, Jiang L (2010) J Mater Chem 20:5095
9. Liu B, Ochiai T, Nakata K, Sakai M, Murakami T, Saito H, Takagi K, Fujishima A (2012) Catal Sci Tech 2:1933
10. Kao L-H, Hsu T-C, Cheng K-K (2010) J Colloid Interface Sci 341:359
11. Fujishima A, Honda K (1972) Nature 238:37
12. Tang J, Durrant JR, Klug DR (2008) J Am Chem Soc 130:13885
13. Yu J, Qi L, Jaroniec M (2010) J Phys Chem C 114:13118
14. Khade GV, Suwarnkar MB, Gavade NL, Garadkar KM (2015) J Mater Sci: Mater Electron 26:3309
15. Armstrong AR, Armstrong G, Canales J, Bruce PG (2005) J Power Sour 146:501
16. Park H, Kim WR, Jeong HT, Lee JJ, Kim HG, Choi WY (2011) Sol Energy Mater Sol Cells Res 95:184
17. Liu L, Chen X (2014) Chem Rev 114:9890
18. Lu XJ, Mou XL, Wu JJ, Zhang DW, Zhang LL, Huang F, Xu FF, Huang SM (2010) Adv Funct Mater 20:509
19. Cargnello M, Gordon TR, Murray CB (2014) Chem Rev 114:9319
20. Li D, Xia Y (2004) Nano Lett 4:933
21. Xu C, Wu J, Desai UV, Gao D (2011) J Am Chem Soc 133:8122
22. Zhuge F, Qiu J, Li X, Gao X, Can X, Yu W (2011) Adv Mater 23:1330
23. Yang S-C, Yang D-J, Kim J, Hong J-M, Kim H-G, Kim I-D (2008) Adv Mater 20:1059
24. Nilsson E, Sakamoto Y, Palmqvist AEC (2011) Chem Mater 23:2781
25. Eun TH, Kim S-H, Jeong W-J, Jeon S-J, Kim S-H, Yang S-M (2009) Chem Mater 21:201
26. Chen H, Zhen Y, Song Y, Jiang L (2008) J Am Chem Soc 130:7800
27. Koo H-J, Kim Y-J, Lee Y-H, Lee W-I, Kim K, Park N-G (2008) Adv Mater 20:195
28. Xiang G, Li T (2010) Chem Commun 46:6801
29. Li Y, Sasaki T, Shimizu Y, Koshizaki N (2008) J Am Chem Soc 130:14755
30. Tan LK, Kumar MK, An WW, Gao H (2010) ACS Appl Mater Interfaces 2:498
31. Formo E, Lee E, Campbell D, Xia Y (2008) Nano Lett 8:668
32. Barbé CJ, Arendse F, Comte P, Jirousek M, Lenzmann F, Shklover V, Grätzel M (1997) J Am Ceram Soc 80:3157
33. Pathak P, Meziani MJ, Castillo L, Sun Y-P (2005) Green Chem 7:667
34. Srinivasn M, White T (2007) Environ Sci Technol 41:4405
35. Wang C-C, Ying JY (1999) J Chem Mater 11:3113
36. Sugimoto T, Zhou X, Muramatsu A (2003) J Colloid Interface Sci 259:53
37. Wang HE, Zheng LX, Liu CP, Liu YK, Luan CY, Cheng H, Li YY, Martinu L, Zapien JA, Bello I (2011) J Phys Chem C 115:10419
38. Yang W, Wan F, Chen Q, Li J, Xu D (2010) J Mater Chem 20:2870
39. Zhong L-S, Hu J-S, Wan L-J, Song W-G (2008) Chem Commun:1184
40. Chen D, Huang F, Cheng Y, Aruso RA (2009) Adv Mater 21:2206
41. Kanie K, Sugimoto T (2004) Chem Commun:1584
42. Nagaveni K, Hegde MS, Ravishankar N, Subbanna GN, Madras G (2004) Langmuir 20:2900
43. Wang CM, Wu H, Chung SL (2006) J Porous Mater 13:307
44. Durupthy O, Bill J, Aldinger F (2007) Cryst Growth Des 7:2696
45. Anuradha TV, Ranganathan S (2007) Bull Mater Sci 30:263
46. Kobayashi M, Petrykin V, Tomita K, Kakihana M (2008) J Ceram Soc Jpn 116:578
47. Jia H, Xiao W-J, Zhang L, Zheng Z, Zhang H, Deng F (2008) J Phys Chem C 112:11379
48. Hayami Y, Suzuki Y, Sagawa T, Yoshikawa S (2010) J Nano Sci Nanotechnol 10:2284
49. Sedghi A, Baghshahi S, Nouri NR, Barkhordari M (2011) Digest J Nanomater Biostruct 6:1457
50. Ding S, Huang F, Mou X, Wu J, Lü X (2011) J Mater Chem 21:4888
51. Tao Y, Xu Y, Pan J, Gu H, Qin C, Zhou P (2012) Mater Sci Eng B 177:1664
52. Mani AD, Raju BR, Ghosal NXP, Sreedhar B, Subrahmanyam C (2013) Chem Eng J 228:545
53. Senna M, Myers N, Aimable A, Laporte V, Pulgarin C, Baghriche O, Bowen P (2013) J Mater Res 28:354
54. Chang Y, Liu X, Cai A, Xing S, Ma Z (2014) Ceram Int 40:14765
55. Roddick-Lanzilotta AD, McQuillan AJ (2000) J Colloid Interface Sci 227:48
56. Schmidt M (2001) Arch Orthop Trauma Surg 121:403
57. Schmidt M, Steinmann SG (1991) J Anal Chem 341:412
58. Chu R, Yan J, Lian S, Wang Y, Yan F, Chen D (2004) Solid State Commun 130:789
59. Bakre PV, Volvoikar PS, Vernekar AA, Tilve SG (2016) J Colloid Interface Sci 474:58
60. Yogambal C, Vizhi RE, Babu DR (2015) Cryst Res Technol 50:22
61. Cheyne RW, Smith TAD, Trembleau L, Mclaughlin AC (2011) Nanoscale Res Lett 6:423
62. Carla E, Giacomelli M, Avena J, De Pauli CP (1996) Langmuir 11:3483
63. Thamaphat K, Limsuwan P, Ngotawornchai B (2008) Kasetsart J (Nat Sci) 42:357
64. Antony KJ, Raj K, Vishwanathan B (2009) Indian J Chem 48A:1378
65. Leofanti G, Padovan M, Tozzola G, Venturelli B (1998) Catal Today 41:207